Role of lee waves in the formation of solid polar stratospheric clouds: Case studies from February 1997

E. Rivière, Nathalie Huret, F. G. Taupin, Jean-Baptiste Renard, Michel Pirre, S. Eckermann, N. Larsen, T. Deshler, Franck Lefèvre, Sébastien Payan, et al.

JOURNAL OF GEOPHYSICAL RESEARCH, VOL. 105, NO. D5, PAGES 6845–6853, MARCH 16, 2000

Role of lee waves in the formation of solid polar stratospheric clouds: Case studies from February 1997

E. D. Rivière,[1] N. Huret,[1,2] F. G.-Taupin,[1] J.-B. Renard,[1] M. Pirre,[1,2] S. D. Eckermann,[3] N. Larsen,[4] T. Deshler,[5] F. Lefèvre,[6] S. Payan,[7] and C. Camy-Peyret[7]

Abstract. Recent theories of solid polar stratospheric clouds (PSCs) formation have shown that particles could remain liquid down to 3 K or 4 K below the ice frost point. Such temperatures are rarely reached in the Arctic stratosphere at synoptic scale, but nevertheless, solid PSCs are frequently observed. Mesoscale processes such as mountain-induced gravity waves could be responsible for their formation. In this paper, a microphysical-chemical Lagrangian model (MiPLaSMO) and a mountain wave model (NRL/MWFM) are used to interpret balloon-borne measurements made by an optical particle counter (OPC) and by the Absorption par Minoritaires Ozone et NO_x (AMON) instrument above Kiruna on February 25 and 26, 1997, respectively. The model results show good agreement with the particle size distributions obtained by the OPC in a layer of large particles, and allow us to interpret this layer as an evaporating mesoscale type Ia PSC (nitric acid trihydrate) mixed with liquid particles. The detection of a layer of solid particles by AMON is also qualitatively reproduced by the model and is interpreted to be frozen sulfate acid aerosols (SAT). In this situation, the impact of mountain waves on chlorine activation is studied. It appears that mesoscale perturbations amplify significantly the amount of computed ClO, as compared to synoptic runs. Moreover, MiPLaSMO chemical results concerning HNO_3 and HCl agree with measurements made by the Limb Profile Monitor of the Atmosphere (LPMA) instrument on February 26 at a very close location to AMON, and explain part of the differences between LPMA measurement and Reactive Processes Ruling the Ozone Budget in the Stratosphere (REPROBUS) model outputs.

1. Introduction

In polar regions, heterogeneous reactions which occur on stratospheric aerosols and on polar stratospheric clouds (PSCs) are a crucial step in chlorine activation responsible for ozone loss [*Solomon et al*, 1986]. The efficiency of those processes depends on three parameters strongly linked to the temperature: particle type, surface area, and chemical composition in the case of liquid particles. Thus the way in which PSCs form is of primary importance. Our knowledge of PSCs formation has evolved over the past few years, particularly concerning solid particle formation. Five types of particles are usually considered: liquid binary aerosols, sulfuric acid tetrahydrate (SAT) particles, type Ia PSC made of nitric acid trihydrate (NAT), liquid type Ib PSC ($H_2SO_4/HNO_3/H_2O$) also named supercooled ternary solution (STS), and type II PSC made of ice particles. Some pathways of solid PSCs formation remain uncertain, especially concerning PSC Ia [*Tolbert*, 1996]. *Tabazadeh et al.* [1994] and *MacKenzie et al.* [1995] suggest that PSC Ia can be formed by freezing of STS. *Zhang et al.* [1996] show that NAT could form by nucleation on preactivated SAT. *Tabazadeh and Toon* [1996] suggest that solid type PSC could form through a metastable dilute HNO_3/H_2O solid phase. Other works point out that PSC Ia could be composed first of metastable nitric acid dihydrate (NAD) particles which could form in a strong warming event [*Tsias et al.*, 1997], and convert later into NAT [*Middlebrook et al*, 1992]. More recent studies suggest that NAT could form by nucleation on ice nuclei [*Biermann et al.*, 1998]. Type II PSC would therefore be the first step in the formation of solid PSCs [*Koop et al.*, 1997]. SAT particle formation was studied from binary solution freezing experiments, although this mechanism does not occur under polar stratospheric conditions [*Clapp et al*, 1997; *Carleton et al.*, 1997], since the droplets are STS at temperatures at which they are supposed to freeze. SAT formation mechanism is therefore still unclear. However, SAT particles could play an important role in PSCs cycle formation: *Koop and Carslaw* [1996] have shown that SAT deliquescence could convert SAT aerosols into STS droplets, which could freeze later to produce solid PSCs [*Iraci et al.*, 1998].

Our knowledge about the temperature at which solid particles are formed has also developed over the last few years. *Koop et al.* [1995] have shown that liquid particles would not freeze above the ice frost point (hereafter T_{ice}). *Koop et al.* [1997] suggest that liquid particles could remain liquid down to 3 K below T_{ice}, while *Carslaw et al.* [1998a] suggest 4 K

[1]Laboratoire de Physique et Chimie de l'Environnement, CNRS, Orléans, France.
[2]Also at Université d'Orléans, Orléans, France.
[3]E. O Hulburt Center for Space Research, Naval Research Laboratory, Washington, D C.
[4]Department of Research, Danish Meteorological Institute, Copenhagen, Denmark
[5]Department of Atmospheric Science, University of Wyoming, Laramie.
[6]Service d'Aéronomie du CNRS, Paris, France
[7]Laboratoire de Physique Moléculaire et Applications, CNRS, Paris, France

Paper number1999JD900908.
0148-0227/00/1999JD900908$09.00

below T_{ice}. This imposes very restrictive conditions for solid particle formation, since at synoptic scale, such temperatures are not usually reached in the Arctic stratosphere. However, mesoscale processes such as mountain-induced gravity waves can generate vertical air motions that are large enough to adiabatically cool the air parcels to 3-4 K below T_{ice} [*Carslaw et al.*, 1998a]. The role of mountain-induced waves (lee waves) on PSC microphysics and chlorine activation has been investigated recently [*Meilinger et al.*, 1995; *Tsias et al.*, 1997; *Carslaw et al.* 1998b, 1999].

In this context, the aim of this paper is to study two cases of particle observation in February 1997 over Kiruna (67.9°N/ 22.1°E), Sweden, which cannot be explained by synoptic scale temperature histories. On February 25, 1997, a balloon-borne optical particle counter (OPC) [*Deshler et al.*, 1993] measured a layer of large particles, while the balloon-borne Absorption par Minoritaires Ozone et NO_x (AMON) [*Renard et al.*, 1996] instrument detected a layer of solid particles on February 26. The Microphysical and Photochemical Lagrangian Stratospheric Model of Ozone (MiPLaSMO), which has been developed to study the chemical composition of the stratosphere (taking into account a detailed PSC model, stratospheric chemistry, and heterogeneous reactions on PSCs), is used to tentatively explain the measurements. The orographic gravity wave model of *Bacmeister et al.* [1994] is also used in this work to investigate the role of mountain waves in the formation of these disturbed layers.

The models used here are described in detail in section 2, then the instruments OPC, AMON, and Limb Profile Monitor of the Atmosphere (LPMA) are presented in section 3. For the two cases considered in this paper, the role of lee waves in the formation of disturbed layers is investigated in sections 4 and 5. In the case of February 26, 1997, the role of mountain waves in chlorine activation is discussed by comparing MiPLaSMO chemical outputs with Reactive Processes Ruling the Ozone Budget in the Stratosphere (REPROBUS) Chemistry Transport Model (CTM) calculations and LPMA measurements of HNO_3 and HCl [*Payan et al.*, 1999].

2. Model Description

2.1. MiPLaSMO

MiPLaSMO is a numerical model, which was developed to study in detail microphysical and chemical processes associated with PSCs. This model describes the evolution of the microphysical, thermodynamical, and chemical properties of an air parcel following an isentropic trajectory. The PSC code and the photochemical code are coupled via heterogeneous chemistry. In this section, the different packages of the model are described.

2.1.1. Trajectory model. MiPLaSMO uses isentropic trajectories as input. Trajectories are calculated [*Knudsen and Carver*, 1994] using European Centre for Medium-Range Weather Forecast (ECMWF) meteorological data with a spatial resolution of 1.125° x 1.125°. They are available every 6 hours. Trajectory data are calculated every 2 hours. Mesoscale perturbations of temperature and pressure can be prescribed along the trajectory.

2.1.2. Microphysical code. The microphysical code was initially developed at the Danish Meteorological Institute by N. Larsen [*Larsen et al.*, 1997]. It describes the time evolution of several kinds of particles: PSC Ia (supposed to be NAT),

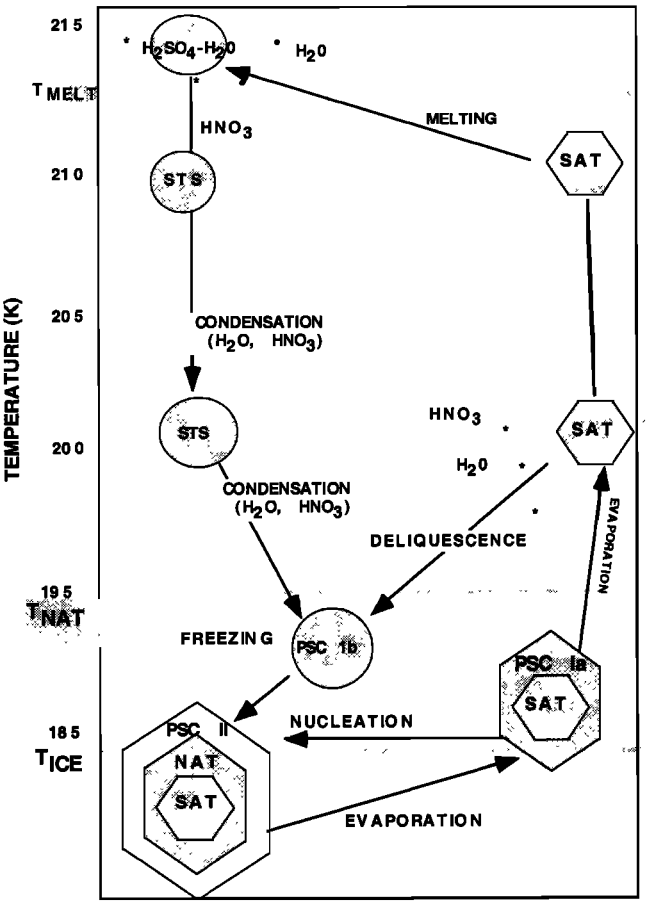

Figure 1. Scheme of PSC formation used in the model as a function of the temperature. Typical values of T_{NAT}, T_{ice} and T_{melt} are indicated.

PSC II, solid sulfuric aerosols supposed to be SAT, and liquid particles. All the particles are distributed in 50 size bins from 0.001 μm to 100 μm. Figure 1 presents the pathways used in this code for particle evolution, as a function of temperature.

As the temperature decreases, the liquid binary aerosols grow as STS by uptake of HNO_3 and H_2O from the gas phase. PSC II particles are the first solid particles to form from freezing of liquid droplets. The process begins at temperatures less than T_{ice} −1 K. According to *Koop et al.* [1997], particles can remain liquid until the T_{ice} −3 K threshold is reached. During this freezing process, the condensed HNO_3 and H_2SO_4 are conserved through the formation of an inner NAT shell surrounding a SAT core in the ice particle. All the sulfuric acid is in the condensed phase. As the temperature warms up, the ice particles evaporate, revealing the NAT core and NAT can evaporates to leave SAT particles. Size evolution of liquid, NAT, and ice particles due to the condensation/evaporation mechanism is taken into account. Heterogeneous nucleation of PSC II on PSC Ia is also considered when T_{ice} is reached. In the model we assume that SAT can return to liquid particles in two cases: when temperatures pass beyond the melting temperature of SAT, or when temperatures go below the temperature of SAT deliquescence [*Koop and Carslaw*, 1996] if no other solid particles exist.

2.1.3. Photochemical code. The chemical code describes the evolution of 41 species of the NO_y, HO_x, Cl_y, O_x, and Br_y

families. It takes into account 112 homogeneous reactions and five heterogeneous reactions on clouds or aerosols. Those heterogeneous reactions are

(R1) $HCl + ClONO_2 \rightarrow Cl_2 + HNO_3$
(R2) $H_2O + ClONO_2 \rightarrow HOCl + HNO_3$
(R3) $N_2O_5 + HCl \rightarrow ClNO_2 + HNO_3$
(R4) $N_2O_5 + H_2O \rightarrow 2\,HNO_3$
(R5) $HOCl + HCl \rightarrow Cl_2 + H_2O$

First-order rate constants k (s^{-1}) for heterogeneous reactions depend on type and surface of particles. They are calculated as follows:

$$k = \gamma\, S\, \bar{v} \quad (1)$$

where S is the total area of a particle type considered for the considered particle type, $\bar{v}$ the mean thermal velocity, and γ the reaction probability. Reaction probability are taken from *De More et al.* [1997], *Carslaw and Peter* [1997], and *Ravishankara and Hanson* [1996].

The numerical scheme used for the chemical code is semi-implicit symmetric (SIS). The nonlinear equations of chemical species evolution are converted into a linear system of equations. A description of this method can be found in the work by *Ramaroson et al.* [1992].

2.2. Mountain-Wave Calculation

Coolings induced by mountain waves are calculated off-line by the Naval Research Laboratory Mountain Wave Forecast Model (NRL/MWFM). It is described by *Bacmeister et al.* [1994]. Extensions of the model to calculate temperature variability are described by *Eckermann and Bacmeister* [1998]. The model relies on a database of dominant topographic mountain ranges with estimation of their height, width, and orientation. Vertical motions induced by the mountain ridge are calculated at each standard pressure level (including 50, 30, and 10 hPa) and every 6 hours by NRL/MWFM. The temperature perturbation is then deduced using adiabatic parcel thermodynamics, since stratosphere mountain wave advection is adiabatic to a good approximation [*Eckermann et al.*, 1998]. The temperature perturbation introduced in MiPLaSMO is deduced from cooling pathways previously calculated by NRL/MWFM. Interpolations are made to the pressures and times of interest. As in *Tsias et al.* [1997], the mesoscale temperature variation is assumed sinusoidal. The amplitude of the sinusoid varies with respect to the maximum cooling computed by the mountain wave model. The period of the oscillation is estimated from the mean time between two consecutive cooling events as forecast by the NRL/MWFM model.

3. Instruments

In the frame of the validation campaign of the Improved Limb Atmospheric Spectrometer (ILAS) instrument on board the ADEOS satellite [*Sasano et al.*, 1999], chemical species and aerosol measurements were performed in early 1997 with balloon-borne instruments from Kiruna, Sweden. Here we present the OPC, AMON, and LPMA instruments which have performed measurements on February 25 and 26.

3.1. Optical Particle Counter

The OPC used for in situ measurements from the balloon-borne gondola measures the number concentration of condensation nuclei ($r > 0.01$ μm) and of optically detectable aerosol ($0.15 < r < 10.0$ μm). The aerosol counter, following an original design by *Rosen* [1964], counts and sizes aerosol particles drawn into a scattering region. The size is determined from measurements of the intensity of scattered white light at 40° from the forward direction using Mie theory and assuming spherical particles with an index of refraction of 1.45 [*Hofmann and Deshler*, 1991].

3.2. AMON Instrument

AMON is a balloon-borne UV-visible spectrometer devoted to nighttime measurements of the stratospheric species O_3, NO_2, and NO_3 [*Naudet et al.*, 1994; *Renard et al.*, 1996]. Aerosol extinction can also be retrieved as a function of the wavelength. Observations are performed using the stellar occultation method, which consists in analyzing the modifications of the spectrum of a setting star induced by absorbing atmospheric species. A reference spectrum is obtained when the star is above the balloon horizon and the balloon is afloat. The transmission spectra are obtained by dividing the observed spectra by the reference spectrum. The retrieval of the slant column densities is performed using a least squares fit between the observed transmission spectra and the spectra calculated using the known cross sections of the absorbing species. The residual in the transmission spectra, after removing the contribution of Rayleigh scattering and the contribution of molecular absorption, is assigned to aerosols. The vertical profiles of the species and of the aerosol extinction are obtained after inversion performed using the onion peeling technique [*Renard et al.*, 1996].

3.3. LPMA Instrument

The LPMA is a remote sensing infrared Fourier transform instrument operating in absorption against the Sun [*Camy-Peyret*, 1995]. With its high spectral resolution and sensitivity, the retrieval of vertical profiles of trace species having stratospheric mixing ratios as small as 0.1 ppbv is possible. A global fit algorithm [*Carlotti*, 1988] associated with an efficient minimization algorithm of the Levenberg-Marquardt type [*Press et al.*, 1992] is used for the retrieval. This retrieval algorithm [*Payan et al.*, 1998] allowed us to retrieve vertical profiles of HCl, HNO_3, and several other stratospheric species from occultation data.

4. Study of February 25, 1997

4.1. OPC Measurements

Observations were performed from Kiruna (67.9°N/22.1°E) on February 25, 1997. The OPC flight started at 0918 UT and ended at 1051 UT. Data were recorded from the ground to 30 km. The aerosol concentration profiles for different size classes are shown in Figure 2. A layer of large particles was observed between 20 and 22 km.

4.2. Initialization of MiPLaSMO

For this case, the initial distribution of particles, typical of background aerosol, is deduced from OPC measurements. The distribution at the desired altitude is obtained by interpolation between two typical distributions of background aerosols observed below and above this altitude. The distribution measured on February 23, 1997 (T. Deshler, unpublished ILAS database, 1997) has been used. These

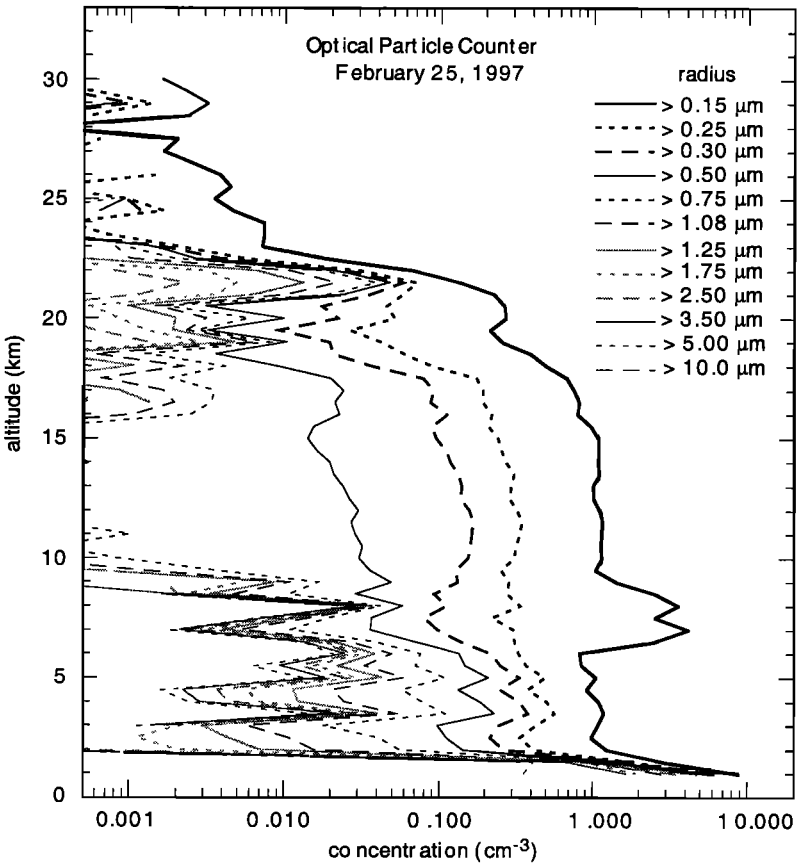

Figure 2. Vertical profiles of aerosol concentration for particles between 0.15 μm and 10 μm from the in situ OPC measurements on February 25, 1997.

measurements have been preferred to those of February 25 because the disturbed layer involving large particles is thinner. This allows a better precision in the interpolation of aerosol parameters. At initialization of the model, particles are assumed to be liquid. Chemical species initialization is taken from REPROBUS 3D CTM [*Lefèvre et al.*, 1998] simulations of the whole winter 1996-1997.

4.3. Synoptic Situation

A 20-day isentropic back trajectory was calculated to obtain the temperature history at the 500 K level, corresponding to 21.5 km (35 hPa), where the largest particles are observed (see Figure 3). At the location of the measurement, the synoptic temperature (192 K) is 5 K over the frost point, and thus, too warm for a PSC formation. Moreover, the coldest temperature reached along this trajectory was 3 K above the ice frost point (120 hours before the measurement). As a consequence, the model does not calculate any solid PSCs, using synoptic-scale temperatures.

4.4. Mesoscale Interpretation

A preliminary study of this case was made by *Huret et al.* [1998], considering a theoretical mesoscale perturbation. The authors have shown that the hypothesis of a mountain wave event could be an explanation to interpret the measurements of February 25, 1997. Here we use mountain-induced wave (lee wave) perturbations predicted by the NRL/MWFM model described above to tentatively explain these observations.

At 500 K the OPC measurements were expressed in terms of concentration as a function of the radius. The back trajectory for February 25 crossed the Scandinavian mountain ranges prior to its arrival at the sampling location (not shown). Two

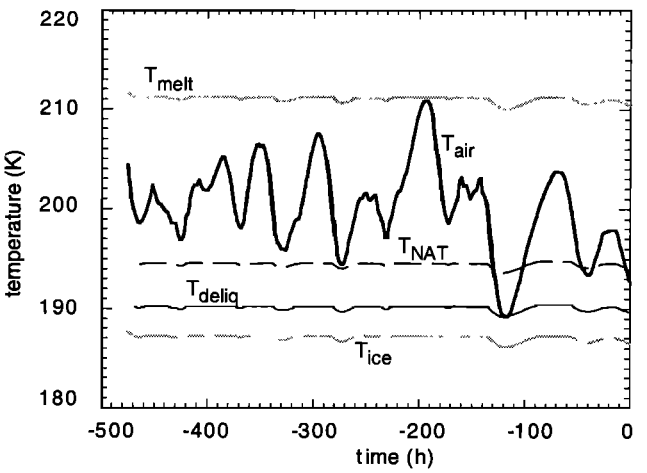

Figure 3. Synoptic temperature time evolution for the 20-day back trajectory (heavy solid line) at the 500 K level for February 25, 1997. Melting temperature of SAT (T_{melt}), temperature of NAT condensation (T_{NAT}), temperature of SAT deliquescence (T_{deliq}), and ice frost point (T_{ice}) are also shown; $t = 0$ corresponds to the time of the measurements.

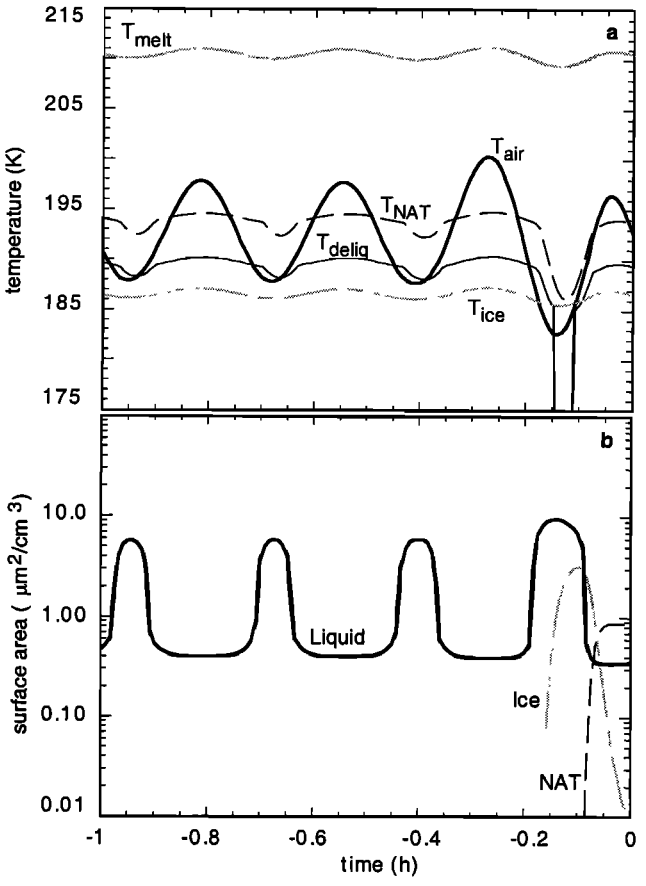

Figure 4. February 25 back trajectory, at 500 K. (a) Mesoscale temperature perturbation 1 hour before the OPC measurements. T_{melt}, T_{NAT}, and T_{ice} are presented (see Figure 3 caption).(b) Surface area time evolution of the particle surface area during the lee wave event shown in Figure 4a.). Liquid particle, NAT, and PSC II total surface area are presented.

hours before the OPC measurements, NRL/MWFM calculations show that the air parcel temperature had been influenced by lee waves, generated by flow over the Scandinavian mountains. The temperature evolution during the last hour of the trajectory is shown in Figure 4a. After a succession of cooling-warming cycles of 5 K amplitude, the maximum cooling induced by the wave is 10 K, which occurs a few minutes before the measurements, and T_{ice} −1 K is reached. Figure 4b shows the evolution of particle surface areas during the lee wave event. When T_{ice} −1 K is reached, a small amount of the largest STS particles freezes into PSC II. Since the T_{ice} −3 K threshold is not reached, some particles remain liquid. Ice particles grow by condensation of water. Then, a warming occurs which makes the ice evaporate, leaving NAT particles. A cooling occurs again, but the temperature stays too high to make NAT grow by condensation of H_2O and HNO_3. SAT begin to appear because of NAT evaporation due to warm temperatures. Finally, the distribution computed at the location of the measurement is composed of liquid particles, NAT, and low concentration of SAT particles. The overall size distribution resulting from model calculations (Figure 5) presents a bimodal structure. This bimodal structure is in good agreement with the measured spectrum of OPC. The first mode centered on a radius of 0.013 μm is mainly composed of liquid particles (with a very small contribution from SAT particles) and the second mode centered on 1 μm is due to NAT particles.

5. Study of February 26, 1997

5.1. Measurements by AMON and LPMA

Observations were also performed from Kiruna, on February 26, 1997. The AMON observations started at 2105 UT and ended at 2211 UT with a balloon float altitude of 31.5 km. The star used for the occultation was Rigel, and 100 spectra were recorded. The latitude and longitude were in the 67.7°-67.0°N and 27.3°-18.5°E ranges, respectively, with tangent point altitudes decreasing from 31.4 to 11.3 km. The LPMA instrument performed a flight from Esrange (68°N/21°E), just before the flight of AMON. Infrared spectra were recorded at sunset during occultation from 1500 UT to 1540 UT. The latitude and longitude ranges for the LPMA occultation measurements were 67.85°-66.87°N and 26.77°-18.78°E, respectively, and so were very close to those of AMON.

5.1.1. Aerosol measurements by AMON. Vertical profiles of aerosol extinction coefficient obtained every 25 nm are shown in Plate 1. Almost all the wavelength dependence of the aerosol extinction coefficients at different altitudes can be fitted using a Mie theory algorithm including a log-log size distribution. The comparison of the aerosols parameters derived from AMON with those of the OPC obtained the day before shows that there is a very good agreement between the two measurements in terms of mean radius. In the altitude range where there is good agreement, the retrieved parameters correspond to background aerosols.

Significant discrepancies from Mie theory occur in a layer between 21 and 23 km in the AMON profile. In this layer the wavelength-dependent extinction is maximum for the larger wavelength and cannot be fitted whatever the refraction index and size distributions used. This result means that the hypothesis of spherical particles used for Mie scattering is not valid. Besides, strong chromatic scintillation was observed

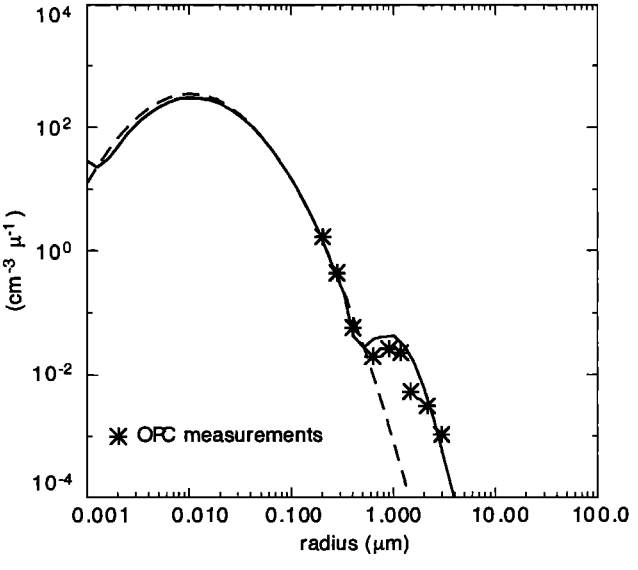

Figure 5. February 25, 1997: size distribution measured by the OPC at the 500 K level (stars) and computed by MiPLaSMO (solid line). Size distribution at initialization used for the simulation is also presented (dashed line).

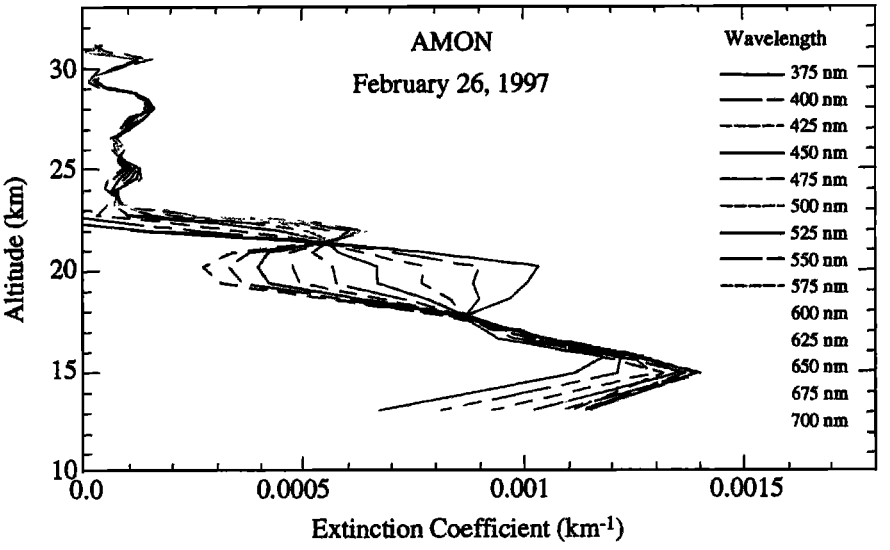

Plate 1. February 26, 1997: vertical profiles of the aerosol extinction coefficient obtained with AMON in the near UV and visible domain (from 375 nm to 700 nm).

by AMON in the layer centered around 22 km. These facts indicate that frozen aerosols are probably present in the corresponding layer.

5.1.2. Chemical trace species measurements of LPMA. At the level of the layer of solid particles measured by AMON, the LPMA infrared remote sensing measurements of HNO_3 and HCl were 11.3±0.6 ppbv and 0.24±0.11 ppbv, respectively.

5.2. Synoptic Situation

The model was initialized in the same way as described in section 4.2. We calculate the temperature history of the air parcel from a 20-day back trajectory at the 520 K level (Figure 6), corresponding to 21.6 km (33 hPa), where the extinction coefficient for the larger wavelength is maximum. The temperature at the location of the measurement is 197 K, which is 11 K above T_{ice} and more than 3 K above T_{NAT}. This is too warm to associate this solid layer with the presence of a PSC. Furthermore, the coldest temperature encountered along the trajectory is more than 4 K above the ice frost point (210 hours before the measurement), so we conclude from the synoptic temperature history that no PSC should have formed because of the warm temperatures. Furthermore, no solid particles are predicted by the model from the synoptic temperature history.

5.3. Mesoscale Interpretation

Mountain-wave model calculations were performed for the two times when the sampled air parcel crossed mountain ranges. On February 26 over the Scandinavian mountains, the maximum perturbation amplitude encountered by the air parcel is 5 K. No solid particles can form, since the lowest temperatures are still 5 K above T_{ice}. However, 92 hours earlier (February 23), the trajectories indicate that this air parcel was again over the Scandinavian mountains and the predicted lee wave activity was much stronger. Figures 7a and 7b show the mesoscale temperatures (computed as before) and the evolution of particle surface areas during this period, respectively, 92 hours prior to sampling by AMON. A 13 K strong cooling was first predicted, which exceeds the supercooling threshold, making all the PSC Ib particles freeze into ice. Then the warming occurs, whereupon the ice evaporates, and NAT begins to appear. NAT also evaporates in this warming, since the temperature is above T_{NAT}. The air cools again to 188 K, 2 K above the frost point, ruling out the possibility of ice formation from heterogeneous nucleation on remaining NAT. The remaining NAT particles evaporate, leaving SAT. The model assumes that SAT can remain frozen until it reaches either the SAT melting temperature or SAT deliquescence temperature. Up to the location of the measurements, those thresholds are never reached at synoptic scale (Figure 6). Moreover, when the air parcel crosses Scandinavia just before the AMON measurements, the aforementioned mesoscale processes induce cooling and warming events, but the maximum cooling induced is more than 2 K above the SAT deliquescence temperature. The maximum warming events are 9 K below the SAT melting

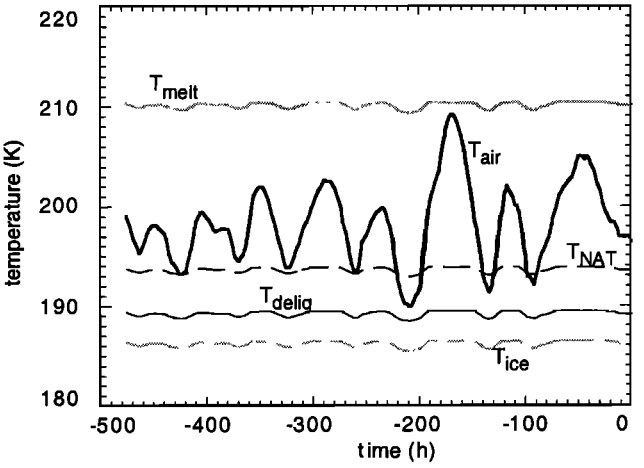

Figure 6. Synoptic temperature time evolution for the 20-day back trajectory (heavy solid line) at the 520 K level for February 26, 1997. See Figure 3 caption for the temperature labels.

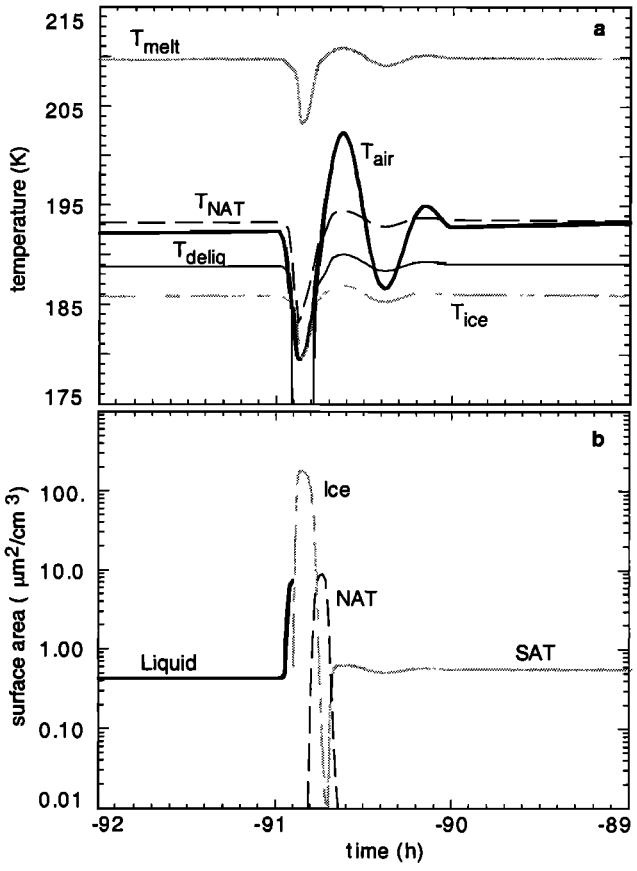

Figure 7. Same as in Figure 4 but for February 26, 1997 at 520 K, 92 hours before the AMON measurements: (a) temperature evolution and (b) time evolution of particle surface area.

temperature, so SAT particles should remain solid. When the air parcel is sampled by the AMON instrument, SAT is the only kind of particle predicted by the model.

Regarding the chemical composition of the atmosphere, the MiPLaSMO microphysical results are compatible with the high HNO_3 concentrations measured by LPMA [*Payan et al.*, 1999] at this altitude, ruling out the presence of a PSC Ia. The nitric acid computed by the model above Kiruna is 11.3 ppbv, while the amount measured by LPMA was between 11.3±0.6 ppbv at this altitude (Figure 8). If a PSC Ia had been observed, the amount of HNO_3 would have been lower, due to condensation of nitric acid and water from the gas phase. The HNO_3 amount computed over Kiruna is more than 1 ppbv greater than the amount used as initialization. This is due to nitric acid production by heterogeneous reactions (R1), (R2), (R3), and (R4) on cloud particles.

The model interpretation of AMON solid particle measurements is then related to a previous mesoscale PSC event, which later evaporation led to the release of frozen sulfuric aerosol particles.

5.4. Implications for Chlorine Activation

In order to evaluate the impact of lee wave activity on chlorine activation, model runs were performed with and without lee waves for the case of February 26, 1997. Time evolution of HNO_3, HCl, $ClONO_2$, and ClO are shown in Figure 8 for cases where lee waves were taken into account or excluded. The initial value (REPROBUS simulations) of ClO_x (i.e., ClO + 2 Cl_2O_2) is equal to 0.2 ppbv, indicating a small chlorine activation of the air parcel. Around 210 hours before the measurements, the synoptic temperature was 3-4 K above the ice frost point (Figure 6), triggering growth of liquid particles by absorption of nitric acid and water. This corresponds to an increase in the chlorine activation as seen by an increase of the calculated ClO_x mixing ratio at night and a calculated decrease of HCl of 0.36 ppbv. This period corresponds to a slight increase of nitric acid of 0.38 ppbv. Indeed, the cumulative effects of large particle size with low temperature and the liquid phase of the particles induce rather large rate constants of heterogeneous reactions and thus, additional chlorine activation. As the first lee wave event occurs over the Scandinavian mountains (at around t = –91 hours), the air parcel is already activated with ClO nighttime values of 0.18 ppbv and ClO_x values of 0.68 ppbv. After this event, differences of more than a factor of 2 appear in daytime ClO concentration between the cases with and without lee

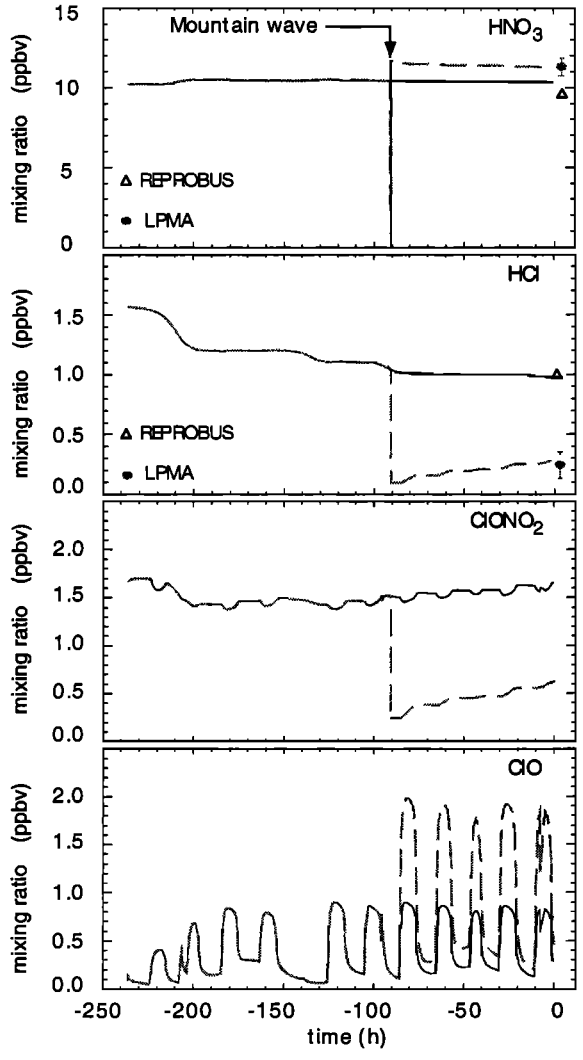

Figure 8. Case study for February 26, 1997, at 520 K. Time evolution for HNO_3, HCl, $ClONO_2$, and ClO mixing ratios, taking into account mountain-wave perturbations starting at about t = - 91 hours (dotted gray line), and excluding them (solid line). HNO_3 and HCl mixing ratios obtained by REPROBUS simulations (triangle) and LPMA measurements (gray circle) at 21 km are also shown.

waves. HCl is almost completely consumed (0.1 ppbv remaining) by heterogereous reactions, and $ClONO_2$ decreases by 1.25 ppbv for the same reason. The $ClONO_2$ loss is in correlation with the nitric acid increase of the same amount due to reactions (R1) and (R2). The contribution of reactions (R3) and (R4) for nitric acid production is negligible because of the very small amount of N_2O_5 in our conditions. It has been verified that for 10-days integration period using synoptic temperature history that REPROBUS and MiPLaSMO results are in rather good agreement (see Figure 8 and Table 1). When lee waves are introduced into the model, the MiPLaSMO values (at 21.6 km at the time of the AMON measurements) of HNO_3 and HCl (11.3 ppbv and 0.30 ppbv, respectively) are in accordance with the measurements of LPMA on February 26, 1997, at 21 km (11.3±0.6 ppbv and 0.24±0.11 ppbv, respectively). Comparisons between MiPLaSMO results and LPMA measurements are summarized in Table 2. Differences between LPMA measurements and REPROBUS simulations could be explained by the fact that REPROBUS is not accounting for mesoscale temperature fluctuations.

6. Conclusion

The aim of the present study was to interpret two sets of measurements performed in February 1997, which cannot be explained by synoptic-scale temperature histories. For this purpose, we have used a Lagrangian chemical and microphysical model (MiPLaSMO) and a mountain wave model (NRL/MWFM). We have shown that, introducing mesoscale temperature perturbations from NRL/MWFM, initialization from the REPROBUS model (chemistry) and OPC measurements (aerosols), with realistic hypotheses about the supercooling threshold for PSCs freezing (i.e., 3 K below the ice frost point), the MiPLaSMO Lagrangian model could produce results in agreement with the layer of large particles observed by the optical particle counter on February 25, 1997. This layer can be interpreted as composed of a small number of NAT particles (PSC Ia) mixed with liquid particles. The maximum temperature amplitude of the lee waves in this simulation was 10 K.

On February 26, the observation of solid particles can be interpreted with MiPLaSMO and the mountain-wave model. Although the mountain-wave model is considered to overestimate the wave amplitude [*Carslaw et al.*, 1999], the 13 K lee wave temperature amplitude used in our model is nevertheless still compatible with the observational case studied by *Carslaw et al.* [1998a]. What is observed could be solid sulfuric acid aerosol, evidence of a previous PSC event.

Table 1. Comparison Between REPROBUS at Two Standard Pressure Levels (21 km and 21.9 km) and MiPLaSMO (21.6 km) Model Results for HNO_3 and HCl.

	HNO_3 (ppbv)	HCl (ppbv)
REPROBUS (LPMA location) (21 km)	9.7	1.00
MiPLaSMO (21 6 km) without lee waves (AMON location)	10 3	0 96
REPROBUS (LPMA location) (21.9 km)	9.6	1.30

Temperature and pressure perturbations are not taken into account

Table 2. Comparison Between LPMA (1530 UT) or AMON (2200 UT) Measurements at 21 and 22 km, and MiPLaSMO Model Results at 21.6 km for HNO_3 and HCl.

	HNO_3 (ppbv)	HCl (ppbv)
LPMA (21 km)	11 3±0.6	0.24±0 11
MiPLaSMO (21.6 km) with lee waves (AMON location)	11.3	0.30
LPMA (22 km)	11.0±0.6	0.45±0.20

Here, mesoscale perturbations due to lee wave are introduced in MiPLaSMO.

This PSC would have been generated by wave perturbations above the Scandinavian mountains, several days before the measurements. Solid aerosol calculations are qualitatively in accordance with the high HNO_3 concentration and the low values of HCl measured on February 26. For this case, we have also shown that even if the air parcel was already chlorine activated before the mesoscale processes occurred, the lee wave activity has significantly amplified the activation process and ClO concentration is more than 2 times greater than without lee waves in daytime conditions. This result is in agreement with the conclusion of *Carslaw et al.* [1998b]. Chemical results of MiPLaSMO are in accordance with HNO_3 and HCl LPMA measurements. Furthermore, mesoscale processes can be an explanation for the differences observed by *Payan et al.* [1999] between the REPROBUS model and LPMA measurements.

Acknowledgments. The authors are grateful to K. Carslaw for providing them a parameterization of SAT deliquescence temperature and to the CNES launching team at Kiruna. The AMON and LPMA flights were performed within the French Programme National de Chimie Atmosphérique and with financial support from CNES and INSU. The Geneva Observatory team is acknowledged for the AMON and LPMA gondola integration and pointing. We would like to thank the NILU database for access to meteorological data, as well as B. Knudsen and F. Fierli for the trajectory calculation program. S. Eckermann acknowledges support from NASA ACMAP grant L68786D.

References

Bacmeister, J.T., P.A. Newman, B.L. Gary, and K.R. Chan, An algorithm for forecasting mountain wave-related turbulence in the stratosphere, *Weather Forecasting, 9*, 241-253, 1994.

Biermann, U.M., J.N. Crowley, T. Huthwelker, G.K. Moortgat, P.J. Crutzen, and T. Peter, FTIR studies on lifetime prolongation of stratospheric ice particles due to NAT coating, *Geophys Res. Lett., 25*, 3939-3942, 1998.

Camy-Peyret, C., Balloon-borne Fourier transform spectroscopy for measurements of atmospheric trace gases, *Spectrochim. Acta, 51A*, 1143-1152, 1995.

Carleton, K.L., D.M. Sonnenfroh, W.T. Rawlins, B.E. Wyslouzil, and S. Arnold, Freezing behavior of single sulfuric acid aerosols suspended in a quadrupole trap, *J. Geophys. Res., 102*, 6025-6030, 1997.

Carlotti, M., Global fit approach to the analysis of limb-scanning atmospheric measurements, *Appl. Opt., 27*, 3250-3254, 1988.

Carslaw, K.S. and T. Peter, Uncertainties in reactive uptake coefficients for solid stratospheric particles, 2, Effect on ozone depletion, *Geophys. Res. Lett., 24*, 1747-1750, 1997.

Carslaw, K.S., M. Wirth, A. Tsias, B.P. Luo, A. Dörnbrack, M. Leutbecher, H. Volkert, W. Renger, J.T. Bacmeister, and T. Peter, Particles microphysics and chemistry in remotely observed mountain polar stratospheric clouds, *J. Geophys. Res., 103*, 5785-5796, 1998a.

Carslaw, K.S., et al., Increased stratospheric ozone depletion due to mountain-induced atmospheric waves, *Nature, 391*, 675-678, 1998b.

Carslaw, K.S., T Peter, J.T. Bacmeister, and S D. Eckermann, Widespread solid particle formation by mountain waves in the Arctic stratosphere, *J Geophys. Res.*, *104*, 1827-1836, 1999.

Clapp, M.L., R.F Niedziela, L.J. Richwine, T Dransfield, R E Miller, and D.R. Worsnop, Infrared spectroscopy of sulfuric acid/water aerosols: Freezing characteristics, *J. Geophys Res.*, *102*, 8899-8907, 1997.

De More, W.B., S.P. Sander, D M. Golden, R.F Hampson, M.J. Kurylo, C.J. Howard, A.R. Ravishankara, C.E. Kolb, and M.J. Molina, Chemical kinetics and photochemical data for use in stratospheric modeling, Evaluation 12, *JPL Publ., 97-4*, 1997.

Deshler, T , B.J. Johnson, and W.R. Rozier, Balloonborne measurements of Pinatubo aerosol during 1991 and 1992 at 41°N. Vertical profiles, size distribution, and volatility, *Geophys. Res. Lett*, *20*, 1435-1438, 1993.

Eckermann, S.D., and J.T. Bacmeister, Global parameterization of gravity wave temperature perturbations for chemical and microphysical models, paper presented at the MEPS workshop, European Commission Environnement and Climate Programme, BMBF POLECAT, DLR, and SPARC, Bad Tölz, Nov. 8-11, 1998.

Eckermann, S.D., D.E. Gibson-Wilde, and J.T. Bacmeister, Gravity wave perturbations of minor constituents: A parcel advection methodology, *J. Atmos. Sci.*, *55*, 3521-3539, 1998.

Hofmann, D.J., and T. Deshler, Stratospheric cloud observations during formation of the Antarctic ozone hole in 1989, *J. Geophys. Res.*, *96*, 2879-2912, 1991.

Huret, N., E.D. Rivière, F. Taupin-Goffinont, and M. Pirre, Lagrangian study of polar stratospheric clouds: The role of lee wave events for clouds formation and chlorine activation at the end of February 1997 close to Kiruna, paper presented at the MEPS workshop, European Commission Environnement and Climate Programme, BMBF POLECAT, DLR, and SPARC, Bad Tölz, Nov. 8-11, 1998.

Iraci, L.T., T.J. Fortin, and M A. Tolbet, Dissolution of sulfuric acid tetrahydrate at low temperatures and subsequent growth of nitric acid trihydrate, *J. Geophys. Res.*, *103*, 8491-8498, 1998.

Knudsen, B.M., and G.D. Carver, Accuracy of the isentropic trajectories calculated for the EASOE campaign, *Geophys. Res Lett.*, *21*, 1199-1202, 1994.

Koop, T. and K. Carslaw, Melting of $H_2SO_4.4H_2O$ particles upon cooling: Implications for polar stratospheric clouds, *Science*, *272*, 1638-1641, 1996.

Koop, T., U. M. Biermann, W. Raber, B. P. Luo, P J. Crutzen and T. Peter, Do stratospheric aerosol droplets freeze above the ice frost point?, *Geophys Res. Lett.*, *22*, 917-920, 1995

Koop, T., K.S. Carslaw and T. Peter, Thermodynamic stability and phase transitions of PSC particles, *Geophys Res. Lett.*, *24*, 2199-2202, 1997.

Larsen, N., B. Knudsen, J. Rosen, N. Kjome, R. Neuber and E. Kyrö, Temperature histories in liquid and solid polar stratospheric cloud formation, *J Geophys Res*, *102*, 23505-23517, 1997.

Lefèvre, F , F Figarol, K S. Carslaw, and T Peter, The 1997 Arctic ozone depletion quantified from three-dimensional model simulations, *Geophys Res. Lett.*, *25*, 2425-2428, 1998

MacKenzie, A.R , M. Kulmala, A Laaksonen, and T Vesala, On the theories of type I polar stratospheric cloud formation, *J Geophys. Res.*, *100*, 11275-11288, 1995

Meilinger, S K , T Koop, B.P Luo, T Huthwelker, K.S. Carslaw, U. Krieger, P J. Crutzen and Th. Peter, Size dependent stratospheric droplet composition in lee wave temperature fluctuations and their potential role in PSC freezing, *Geophys Res Lett.*, *22*, 3031-3034, 1995

Middlebrook, A.M., et al , Formation of model polar stratospheric cloud film, *Geophys Res. Lett*, *19*, 2417-2420, 1992.

Naudet, J P , C Robert, and D. Huguenin, Balloon measurements of stratospheric trace species using a multichanel UV-visible spectrometer, proceedings of the 14th ESA symposium on European rocket and balloon programs researched, Montreux, *European Space Agency Spec. Publ.* 355, 165-168, 1994

Payan, S , C Camy-Peyret, P Jeseck, T. Hawat, G. Durry, and F Lefèvre, First simultaneous HCl and ClONO2 profile measurements in the Arctic vortex, *Geophys Res Lett*, *25*, 2663-2666, 1998

Payan, S , C. Camy-Peyret, P Jeseck, T Hawat, M. Pirre, J.-B Renard, C. Robert, F. Lefèvre, H Kansawa, and Y. Sasano, Diurnal and nocturnal distribution of stratospheric NO_2 from solar and stellar occultation measurements. comparison with models and ILAS satellite measurements, *J. Geophys. Res* , *104*, 21,585-21,593, 1999.

Press, W H., S A. Teukolsky, W T Vetterling, and B.P. Flannery, *Numerical Recipes in Fortran*, 2nd ed , 963 pp , Cambridge Univ. Press, New York, 1992

Ramaroson, R.A , M. Pirre, and D Cariolle, A box model for on-line computation of diurnal variation in a 1-D model Potential for application in multi-dimentionnal cases, *Ann. Geophys* , *10*, 416-428, 1992

Ravishankara, A R., and D R Hanson, Differences in the reactivity of type I polar stratospheric clouds depending on their phase, *J Geophys Res.*, *101*, 3885-3890, 1996

Renard, J B., M Pirre, C. Robert, G. Moreau, D Huguenin, and J.M Russell III, Nocturnal vertical distribution of stratospheric O_3, NO_2 and NO_3 from balloon measurements, *J. Geophys. Res* , *101*, 28,793-28,804, 1996

Rosen, J M., The vertical distribution of dust to 30 km, *J Geophys. Res* , *69*, 4673-4676, 1964.

Sasano, Y , M Susuki, T Yokota, and H Kanzawa, Improved Limb Atmospheric Spectrometer (ILAS) for stratospheric ozone layer measurements by solar occultation technique, *Geophys Res Lett*, *26*, 197-200, 1999.

Solomon, S , R R Garcia, F S. Rowland, and D J. Wuebbles, On the depletion of the Antarctic ozone, *Nature*, *321*, 755-758, 1986

Tabazadeh, A., and O. B. Toon, The presence of metastable HNO_3/H_2O solid phases in the stratosphere inferred from ER 2 data, *J Geophys Res* , *101*, 9071-9078, 1996

Tabazadeh, A., R P. Turco, K. Drdla, M.Z Jacobson, and O B Toon, A study of Type I polar stratospheric cloud formation, *Geophys Res Lett.*, *21*, 1619-1622, 1994

Tolbert, M. A , Polar clouds and sulfate aerosols, *Science*, 272, 1597,1996.

Tsias, A., A J Prenni, K. S Carslaw, T P. Onasch, B. P. Luo, M. A. Tolbert, and T. Peter, Freezing of polar stratospheric clouds in orographically induced strong warming events, *Geophys. Res. Lett* , *24*, 2303-2306, 1997

Zhang, R , M T Leu, and M.J. Molina, Formation of polar stratospheric clouds on preactivated background aerosols, *Geophys. Res Lett.*, *23*, 1669-1672, 1996.

C Camy-Peyret and S Payan, Laboratoire de Physique Moléculaire et Applications, CNRS, 4 Place Jussieu, Bte 76, 75252 Paris cedex 05, France (camy@ccr jussieu.fr, payan@ccr.jussieu.fr)

T Deshler, Department of Atmospheric Science, University of Wyoming, 16th and Gibbon, Laramie, WY 82071 (deshler@grizzly uwyo.edu)

S D. Eckermann, E O. Hulburt Center for Space Research, Naval Research Laboratory, Mail code 7641, Washington, DC 20375. (eckerman@ismap4.nrl navy.mil)

N. Huret, M Pirre, J -B. Renard, E. D. Rivière, and F. G.-Taupin, Laboratoire de Physique et Chimie de l'Environnement, CNRS, 3A, Avenue de la Recherche Scientifique, 45071 Orléans cedex 2, France. (nhuret@cnrs-orleans fr, mpirre@cnrs-orleans.fr, renard@cnrs-orleans.fr, riviere@cnrs-orleans fr, goffinon@cnrs-orleans fr)

N Larsen, Department of Research, Danish Meteorological Institute, Lyngbyvej 100, DK-2100, Copenhagen, Denmark. (nl@dmi dk)

F. Lefèvre, Service d'Aéronomie du CNRS, Université Pierre et Marie Curie, BP 102, 4 place Jussieu, 75252 Paris cedex 05, France. (franck.lefevre@aero jussieu fr)

(Received May 4, 1999, revised July 19, 1999;
accepted August 23, 1999.)